



## A review and statistical study of existing hysteresis models for cementitious materials

Zhidong Zhang, Mickaël Thiery, Véronique Baroghel-Bouny

### ► To cite this version:

Zhidong Zhang, Mickaël Thiery, Véronique Baroghel-Bouny. A review and statistical study of existing hysteresis models for cementitious materials. *Cement and Concrete Research*, 2014, 57, pp.44 - 60. 10.1016/j.cemconres.2013.12.008 . hal-01622015

**HAL Id: hal-01622015**

**<https://enpc.hal.science/hal-01622015>**

Submitted on 23 Oct 2017

**HAL** is a multi-disciplinary open access archive for the deposit and dissemination of scientific research documents, whether they are published or not. The documents may come from teaching and research institutions in France or abroad, or from public or private research centers.

L'archive ouverte pluridisciplinaire **HAL**, est destinée au dépôt et à la diffusion de documents scientifiques de niveau recherche, publiés ou non, émanant des établissements d'enseignement et de recherche français ou étrangers, des laboratoires publics ou privés.

# A review and statistical study of existing hysteresis models for cementitious materials

Zhidong ZHANG, Mickaël THIERY, Véronique BAROGHEL-BOUNY

*Université Paris-Est, IFSTTAR, MaS<sub>2</sub>/FM<sup>2</sup>D, F-77447 Marne la Vallée, France*

---

## Abstract

Hysteretic behavior of water vapour sorption isotherms (WVSIs) has been widely recognized as one of main factors which can significantly affect moisture transport within building materials exposed to natural weather conditions. Due to the lack of experimental data for validation, there are few studies about hysteresis models in the field of cementitious materials. In this paper, a detailed review of hysteresis models has been presented. Models which have been initially developed for water transport in soils and sands have been selected, including the conceptual and empirical models. The comprehensive comparisons with experimental data have been performed for cement pastes and concretes. It enables to conclude a set of best models for prediction of WVSIs and their hysteresis. Comparison results show that for the prediction of the first scanning curves, available hysteresis models (either conceptual or empirical) perform similarly. However, studied empirical models yield *pumping errors* for the secondary or higher order scanning loops. A multi-level hysteresis modelling has been proposed as well. Evaluations and recommendations for use of this multi-level modelling method have been provided for an application purpose of compared models.

**Keywords:** cementitious materials, water vapour sorption isotherms, hysteresis, scanning curves, statistics

---

## 1. Introduction

The durability of reinforced concrete structures and their service life are closely related to the simultaneous occurrence of many physical and chemical phenomena. These phenomena are diverse in nature, but in common they are dependent on the moisture properties of the material. Therefore, the prediction of the potential degradation of cementitious materials requires the study of the movement of liquid-water and gas diffusion in the material which is considered as a porous medium. For the modelling of moisture transport in this kind of materials, such as the continuum model proposed in [1], the WVSIs, describing the relationship between relative humidity RH (or capillary pressure  $P_c$ ) and water content  $\theta$  (or degree of saturation  $S$ ), are used to address the equilibrium between liquid-water and vapour. A group of typical WVSIs are illustrated in Fig. 1, which contains two main isotherms (adsorption  $AB$  and desorption  $BA$ ) and several scanning curves (the first and secondary wetting scanning curves  $CB$  and  $EB$ , and the first scanning curve in drying  $DE$ ).

In experiments, only a limited number of WVSI loops can be measured. Nevertheless, in natural conditions, concrete structures undergo arbitrary drying and wetting cycles. Thus, using relevant models to predict these curves for cementitious materials is necessary for modelling of moisture transport.

A main characteristic of WVSIs is their hysteretic behavior, referring to the different water content at the same RH value (see the differences between two main curves in Fig. 1). The most studied reasons of moisture hysteresis in porous media, such as soils and sands, are the “ink-bottle” effect (*e.g.*, [2]), the variation in liquid-solid contact angle (*e.g.*, [3]) and the difference of spatial connectivity of pores during the drying and wetting processes. For cementitious materials, the characteristics of the hysteretic behavior might be different to soils or sands because cementitious materials contain a wider range of magnitude of pore sizes (from gel pores to capillary pores) [4]. Experiments showed that in the low RH range ( $\leq 33\%$ , according to [5]), hysteresis between the desorption and adsorption isotherms is much smaller than in the high RH range. This results from the nanostructure of C-S-H [6], which is not found in soils and sands.

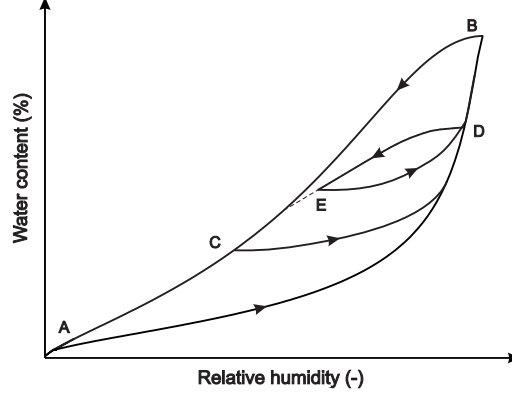


FIGURE 1: Schematic representation of WVSIs. The main desorption curve ( $BA$ ), the main adsorption curve ( $AB$ ), the first scanning curve in drying ( $DE$ ), the first scanning curve in wetting ( $CB$ ) and the second scanning curve in wetting ( $EB$ ) are illustrated.

Although pore systems of different types of materials are different, it is of interest to test whether the hysteresis models from soil science are also applicable to cementitious materials, as there are few studies on the hysteresis behavior of such materials. Carlier *et al.* [7] evaluated different closed-forms of analytical WVSIs expressions used in soil science. The authors concluded that all models were able to correctly represent the desorption isotherms for mortars and concretes. Recently, Johannesson *et al.* [8] and Derluyn *et al.* [9] have used hysteresis models to investigate hysteretic effects on moisture behavior of cementitious materials.

The main objective of this paper is to properly describe WVSIs of cementitious materials, including their hysteresis, by using mathematical formulas. After a review of the development of hysteresis models, we will focus on the comparison of commonly-used WVSIs and hysteresis models that are mainly collected from soil science. Available experimental data in the literature for cement pastes and concretes will be used to verify these models. The main features and recommendations will be given in the last part according to a proposed multi-level modelling of hysteresis.

## 2. Review of hysteresis models

The first documented description of the relation  $P_c - \theta$  in porous media was provided by Haines [10]. After that, the hysteretic behavior of this relation was recognized and several models had been developed to predict hysteresis. Those models can roughly be classified into two groups : conceptual and empirical models [11, 12].

The conceptual models are mainly known as *independent* or *dependent* domain models, which usually employs *distribution diagrams* to demonstrate the theory. They assume that a domain is made up of groups of pores in a porous material. Poulouvassilis was one of the first to adopt the independent domain models from magnetism science to the research of water transport in porous media [13]. This theory, including Preisach space and Néel's diagram, was developed and improved by Preisach [14], Néel [15], Everett [16, 17], *etc.* However, it was reported that those models showed discrepancies with experimental data [18–20]. Hence, researchers tried to modify and develop new models for porous materials. Based on the *similarity hypothesis* proposed by Philip [21], Mualem [22, 23] introduced the simplified independent domain models. The basic idea of Mualem's independent models is that no interactions between those pores are considered. In other words, each pore is independent of its neighbours. So the drying or wetting of the pore system is only determined by the pore necks and pore bodies. Two normalized variables,  $\bar{r}$  and  $\bar{\rho}$  varying from 0 to 1, are used to represent the normalized radii of pore necks and pore bodies, respectively. When  $\bar{r}$  (or  $\bar{\rho}$ ) = 1, it corresponds to the minimum capillary pressure  $P_c^{\min}$  and  $\bar{r}$  (or  $\bar{\rho}$ ) is 0 when  $P_c = P_c^{\max}$ . At a given capillary pressure,  $\theta$  can be obtained by integration of the pore water distribution function  $f(\bar{r}, \bar{\rho})$ . In independent domain models,  $f(\bar{r}, \bar{\rho})$  is formulated by the combined contribution of two independent pore water distribution functions  $h(\bar{r})$  and  $l(\bar{\rho})$ , which describe the radii of pore necks and pore bodies, respectively.

$$\theta = \int \int f(\bar{r}, \bar{\rho}) d\bar{r} d\bar{\rho} = \int l(\bar{\rho}) d\bar{\rho} \int h(\bar{r}) d\bar{r} \quad (1)$$

A rectangle diagram was proposed by Mualem (see Fig. 2) [23] to depict how the independent domain model works. The horizontal axis represents the water distribution function  $h(\bar{r})$  and the vertical axis represents the function  $l(\bar{\rho})$ . At equilibrium, the capillary pressure throughout the pore network is constant [24], either for pore necks or in pore bodies. So,  $h(\bar{r})$  and  $l(\bar{\rho})$  always change at the same capillary pressure, which is illustrated as the diagonal line in Mualem's diagram (see Fig. 2). Hence, the diagram is able to describe the total water distribution ( $f(\bar{r}, \bar{\rho})$ ) through the product of  $h(\bar{r})$  and  $l(\bar{\rho})$ . The water content at  $P_c$  during the wetting process is obtained by integrating the water distribution function from the smallest pore size (at  $P_c^{\max}$ ) to current pore size (at  $P_c$ ) :

$$\theta_w(P_c) = \int_0^{\bar{\rho}(P_c)} l(\bar{\rho}) d\bar{\rho} \int_0^1 h(\bar{r}) d\bar{r} \quad (2)$$

To formulate water content clearly and to avoid using integral forms, two cumulative pore water distribution functions were introduced instead of the integrations for each axis [22].

$$L(P_c) = \int_0^{\bar{\rho}(P_c)} l(\bar{\rho}) d\bar{\rho} \quad H(P_c) = \int_0^{\bar{r}(P_c)} h(\bar{r}) d\bar{r} \quad (3)$$

According to Mualem's diagram,  $L(P_c^{\max}) = 0$ ,  $L(P_c^{\min}) = \theta^{\max}$  (maximum water content), and  $H(P_c^{\max}) = 0$ ,  $H(P_c^{\min}) = \theta^{\max}$ . Hence, Eq. (2) can be rewritten as :

$$\theta_w(P_c) = \theta^{\max} L(P_c) \quad (4)$$

The expression of water content during the drying process is obtained in a similar manner by an integration of Mualem's diagram.

$$\begin{aligned} \theta_d(P_c) &= \int_0^{\bar{\rho}(P_c)} l(\bar{\rho}) d\bar{\rho} \int_0^1 h(\bar{r}) d\bar{r} + \int_{\bar{\rho}(P_c)}^1 l(\bar{\rho}) d\bar{\rho} \int_0^{\bar{r}(P_c)} h(\bar{r}) d\bar{r} \\ &= \theta_w(P_c) + [\theta^{\max} - \theta_w(P_c)] H(P_c) \end{aligned} \quad (5)$$

From Eq. (5), we get the expression of  $H$  as follows :

$$H(P_c) = \frac{\theta_d(P_c) - \theta_w(P_c)}{\theta^{\max} - \theta_w(P_c)} \quad (6)$$

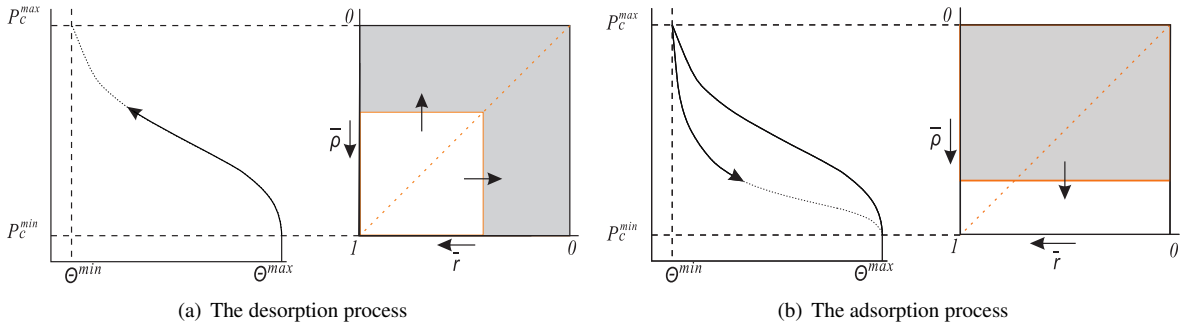


FIGURE 2: Schematic representation of Mualem's diagram [23]. The gray domain represents completely-filled pores and the blank domain stands for fully-dried pores.

If both main isotherms are known ( $\theta_d(P_c)$  and  $\theta_w(P_c)$ ), functions  $H$  and  $L$  can be determined easily by using Eqs. (4) and (6). Then, they are used to calculate scanning loops.

The assumption of *independent* domain means that the pore systems are fully-dried or fully-wet along with the changes of the pressure. Following the research of Topp [19], Mualem and Dagan [25] adjusted the water distribution function (see Eq. 1) by adding two weighting functions ( $p_d \leq 1$  and  $p_w \leq 1$ ).

$$\theta = \int \int p_d(\bar{r}, \bar{\rho}, \theta) p_w(\bar{r}, \bar{\rho}, \theta) f(\bar{r}, \bar{\rho}) d\bar{r} d\bar{\rho} \quad (7)$$

where  $p_d$  represents the volumetric ratio of the actually dried pores to pores supposed to be dried in the independent domain theory. Similarly,  $p_w$  is the ratio for the wetting process. Introducing these two weighting functions implies that the interactions between pores and their neighbours have been considered. This is the basic idea of the *dependent* domain models.

Through a comparison with experimental data, Mualem and Dagan [25] found that  $p_d$  played the major role during both drying and wetting processes, while the effect of  $p_w$  could be neglected ( $p_w = 1$ ). Obviously,  $p_d$  is the key factor for Mualem's dependent models. Various methods attempting to determine  $p_d$  have been reported in the literature [26–28].

The empirical models, which have been applied to the modelling of moisture transport in building materials (*e.g.*, [8]), are developed based on fitting the shapes of experimental WVSIs. Normally, an empirical was proposed without physical meanings. In the literature, there are a number of the empirical models, such as linear models (*e.g.*, [29]), slope models (*e.g.*, [30]) and scaling-down models (*e.g.*, [31]). Initially, they were developed for one type of porous medium (such as soils and sands) and not based on the physical representation of hysteresis. This paper has chosen recently developed and easy-to-apply empirical models which can provide reasonable fitting results for experimental curves of cementitious materials. Such models usually have one or two parameters that need to be determined from experimental data. For example, Li [32] proposed an incremental relation to calculate hysteresis, with one parameter controlling the shape of the curve. In the methods introduced by Wei *et al.* [33] and Nyman *et al.* [34], parameters are used to initialise the slope of the scanning curves.

### 3. Adopted comparison strategy

A strategy of comparison of models for WVSIs and hysteresis to experimental data is introduced. Statistical analysis tools will be presented.

#### 3.1. Procedures of comparisons

According to the availability of experimental data, the normal procedure for the calculation of hysteresis is like as follows :

- If the experimental data for both main adsorption and desorption branches are measured, a model is needed to fit them, and then another model can be used to predict scanning curves ;
- If only one main branch is measured, the other one has to be determined by means of a model, and then scanning curves can be predicted by another model.

Based on above procedure, a multi-level modelling of hysteresis is proposed in Table 1. It depends on the number of available experimental data. This number decreases from Level 1 to Level 3. It may lead to different levels of prediction accuracy, which will be revealed through comparisons in this study.

Table 1 indicates that a complete set of hysteresis models consists of three parts : ① models to fit two main sorption isotherms ; ② models to determine one main sorption isotherm on the basis of the other measured main branch ; ③ models to predict scanning loops. In next sections, hysteresis models will be compared following these three stages.

#### 3.2. Data collection

In order to test the performance of the hysteresis models, measured WVSIs were collected from the literature. The requirements for data collection are :

- 1) The collected data contain at least both main desorption and main adsorption isotherms. It is better if some scanning curves have been measured.
- 2) The number of measurement data for each isotherm must be larger than the number of undetermined parameters in models.

WVSIs can be measured by different methods. The saturated salt solution method is a common gravimetric method in which the RH is controlled by saturated salt solution in a small volume, such as in a desiccator. The mass of

a specimen decreases (during desorption) or increases (during adsorption) until equilibrium (mass stabilization) is reached. Other methods, such as dynamic vapour sorption (DVS) [35, 36], use a small specimen, usually less than 1 g, and a microbalance to monitor mass changes. The advantage of this kind of instruments is that the entire desorption and adsorption loop can be measured in one month or less, more rapidly than with the saturated salt solution method, for which a method can take many months and even years. However, a potential problem with small specimens is that they cannot contain aggregates. Measurements probably quantify only the sorption behavior for the paste in concrete or mortar, rather than the global sorption behavior of the material. For instance, the influence of paste-aggregate interfacial transition zone on the sorption is not investigated in this method. This may lead to different measurement results. Another risk is that small specimens can be carbonated quickly during the preparation.

The studied experimental data are gathered in Table 2 from [5] measured by the saturated salt solution method. These data can meet the above-mentioned comparison requirements very well. All materials are made from the same OPC cement (CEM I 52.5, according to EN 197-1 European standard). They include ordinary and high performance hardened cement pastes and concretes. Water-to-cement ratios range from 0.2 to 0.6. High performance materials are Concrete2 and Paste2, which contain 10% of silica fume to cement in weight. In order to reach chemical stability before the measurements, materials were sealed curing for at least 6 months for concretes and 2 years for cement pastes. Then, cement pastes were crushed into small specimens with masses of about 8 g. Because aggregates have no influence on the sorption process [5], concrete specimens were cut into thin slices, 2 or 3 mm thickness with mass between 20 and 100 g. Measurements started from desorption at RH = 100%, decreasing step-by-step to RH = 3%, considered as the dry reference state. Then, RH increased stepwise to 100% to obtain the adsorption isotherm. To reduce the variations of RH during the measurements as well as the carbonation risk, only a small hole on the top of the desiccator is open for weighing. Besides, the equilibrium state for each RH step was carefully defined as that the mass change is less than 0.001 g after one month. At least three specimens were measured individually to determine one point on the sorption curve.

### 3.3. Comparison criteria

For the fitting of the main sorption isotherms, all parameters in the models are optimized to fit the experimental curves using a nonlinear least squared optimization procedure, which aims to minimize the sum of the squares of the errors.

Two kinds of statistical criteria have been used to evaluate the accuracy of the modelling results in the literature, the coefficient of determination ( $R^2$ ) and a differential residual-based error metrics (see [7, 11]).  $R^2$  is defined as the ratio between the dispersion predicted by the model and the total dispersion of the measured data [11].

The accuracy of fitting (or prediction) is related to the number of parameters used in a model. More parameters usually yields a higher  $R^2$  value, but low robustness and low sensitivity to parameters. To take the effect of the number of parameters into account, we use an adjusted  $R^2$  instead of  $R^2$  [7] :

$$R_{adj}^2 = \frac{(n-1)R^2 - (m-1)}{n-m} \quad (8)$$

where  $m$  is the number of parameters,  $n$  is the number of measured data. Equation (8) implies that  $R_{adj}^2 < R^2$  when  $m > 1$ ,  $R_{adj}^2 = R^2$  when  $m = 1$  and  $R_{adj}^2 > R^2$  when  $m = 0$ . The latter case shows the advantage of using a non-undetermined parameter model.

The other statistical criterion is known as the normalized mean error (NME) :

$$\text{NME} = \frac{1}{n} \sum_{i=1}^n \frac{|S_i^{pr} - S_i^{ms}|}{S_i^{ms}} \quad (9)$$

where  $S_i^{ms}$  and  $S_i^{pr}$  are measured and fitted (or predicted) values, respectively. Notice that the absolute value is used in Eq. (9). It can avoid the cancellation of positive and negative residuals. If the value of NME is close to 0, it indicates a better result.

### 3.4. Data pretreatment

WVSIs measured by experiments are generally RH- $\theta$  relation, but for calculation purpose, models usually need  $P_c - \theta$  or  $P_c - S$ . To get a unified relation, the RH- $S$  relation is used to display fitting or prediction results. The

following equations are employed for transformations. From  $\theta$  to  $S$ , the normalized equation is :

$$S = \frac{\theta - \theta_r}{\theta^{\max} - \theta_r} \quad (10)$$

where  $\theta_r$  is the water content at dry reference state.

From RH to  $P_c$ , Kelvin's equation is used :

$$P_c = -\frac{\rho_l RT}{M_v} \ln RH \quad (11)$$

where  $\rho_l$  is liquid-water density ( $\text{kg} \cdot \text{m}^{-3}$ ),  $R = 8.314 \text{ J} \cdot \text{K}^{-1} \cdot \text{mol}^{-1}$  is the gas constant,  $T$  is the absolute temperature (K).  $M_v$  is the molar mass of water molecule ( $\text{kg} \cdot \text{mol}^{-1}$ ) and RH is a fraction in Eq. (11).

#### 4. Main isotherms fitting models

Numerous models have been proposed to fit the main branches of WVSIs. Each of these equations is applicable to one or several groups of materials (*e.g.*, sands and soils). Models were selected in this research primarily based on whether they can fit both desorption and adsorption isotherms for cementitious materials.

On the whole, two types of methods to fit WVSIs can achieve our purpose. They are uni-modal and multi-modal models. As the name suggests, uni-modal models assume that the material consists of one pore system. Thus, a simple single equation can satisfactorily fit experimental data. In studies of Carlier *et al* [7], the Kosugi model (K) [37] seems to be the better one for the fitting of the main desorption isotherm. Besides, the van Genuchten's model [38], including two-parameter (VG2) and three-parameter (VG3) versions, will be compared. The former version has been used in studies of concretes [39, 40]. Two more models (Feng and Fredlund's model (FF) [41] and Fredlund and Xing's model (FX) [42]) performing well in soil science will be validated for cementitious materials. Multi-modal models consider that there are two or even more pore systems in the material [43]. This consideration can improve the fitting accuracy. A brief description of each selected model will be presented below.

##### 4.1. The Feng and Fredlund's model (FF) [41]

The FF model is an empirical relationship which was used to fit desorption and adsorption curves of a ceramic material [41]. A simple equation is used in this model.

$$S = \frac{a_F}{a_F + P_c^{b_F}} \quad (12)$$

Two parameters ( $a_F$  (Pa) and  $b_F$ ) in Eq. (12) need to be determined. The research performed in [44] showed that this curve-fitting equation is most applicable for low swelling materials (*e.g.*, clay loam).

##### 4.2. The van Genuchten's model [38]

Van Genuchten [38] proposed an  $S$ -shaped curve equation :

$$S = \left[ 1 + \left( \frac{P_c}{a_v} \right)^{n_v} \right]^{-m_v} \quad (13)$$

where  $a_v$  (Pa),  $m_v$  and  $n_v$  are three undetermined parameters. In addition, van Genuchten [38] suggested  $m_v = 1 - 1/n_v$  to simplify Eq. (13) and a two-parameter equation was obtained.

##### 4.3. The Fredlund and Xing's model [42] (FX)

When Fredlund and Xing [42] studied the pore size distribution on the basis of the VG2 model, they found that this model was not suitable in the high capillary pressure region. The authors introduced a modified pore size distribution function. Integration of this function yielded a new equation :

$$S = \left[ \ln \left[ e + \left( \frac{P_c}{a_X} \right)^{n_X} \right] \right]^{-m_X} \quad (14)$$

where  $e$  is the Euler number (a mathematical constant).

#### 4.4. The Kosugi's model [37]

Using a lognormal pore size distribution, Kosugi [37] deduced the following expression :

$$S = Q \left( \sigma^{-1} \ln \frac{P_c}{P_{cm}} \right) \quad (15)$$

where  $P_{cm}$  (Pa) is the capillary pressure related to the medium pore radius.  $\sigma$  is the standard deviation of log-transformed pore radii and is related to the width of the pore size distribution. If the pore size distribution is unknown,  $P_{cm}$  and  $\sigma$  have to be obtained by fitting experimental sorption isotherms. In Eq. (15),  $Q$  denotes the complementary normal distribution function, which is defined as :

$$Q(x) = (2\pi)^{-1/2} \int_x^\infty \exp\left(-\frac{x^2}{2}\right) dx \quad (16)$$

#### 4.5. The multi-modal model

The generalized form of multi-modal models is written as :

$$S = \sum_{i=1}^N w_i S_i(P_c) \quad (17)$$

where  $N$  is the number of pore systems and  $w_i \in [0, 1]$  ( $\sum_i^N w_i = 1$ ) is a weighting factor characterizing pore system  $i$  and  $w_i$  represents the water content contribution of pore system  $i$  to the total water content in the material. If  $N = 2$ , Eq. (17) becomes a bi-modal model. One well-known bi-modal model was proposed by Durner [43], adopting VG2 equation for each pore system.

#### 4.6. Comparison results and discussion

All materials in the collected database have been fitted by above models. Two statistical criteria  $R_{adj}^2$  and NME for the fitting of the two main sorption isotherms are provided in Figs. 3 and 4. Results of two materials (Paste2 and Paste3, representing high performance and ordinary materials) are illustrated in Figs. 6 and 5. Overall, all models provide satisfactory fitting results (mean  $R_{adj}^2 > 0.98$ ). The bi-modal model [43] shows better fitting results than uni-modal models. For all models, the fitting of the adsorption isotherm is better than the fitting of the desorption isotherm.

Concerning uni-modal models, they show a non-physical behavior since the adsorption curves intersect the desorption curves at the low RH (around 0.05 in two examples) for some materials (see the enlarged figures in Figs. 5 and 6 for Paste2 and Paste3, respectively). This phenomenon is not consistent with the experimental data. But for the FX and VG3 models, this behavior is not as significant as for the other two-parameter models (see the enlarged figures in Fig. 6). Both these models show better fitting results than other uni-modal models (see values of  $R_{adj}^2$  and NME in Figs. 3 and 4), either in desorption or in adsorption isotherms. This suggests that these three-parameter models can be used for a variety of cementitious materials. Moreover, one can remark that the widely-used VG2 model [38] does not perform better than other models (see Figs. 3 and 4). Results also show that no selected model can simulate the sudden drop of the desorption isotherms from 44% to 33% RH (see Fig. 6). This drop may be due to measured water content in capillary pores changing to in C-S-H pores as emphasised in reference [5].

Mean values of  $R_{adj}^2$  for the bi-modal model are higher than 0.99 for both desorption and adsorption isotherms and values of NME are close to 0. For Paste3, the bi-modal model roughly shows the same shape as the ones described with other models (see Fig. 6a). For Paste2, this model performs much better in higher RH range, while the predicted desorption isotherm does not reach  $S=0$  at RH=0. This is clearly an non-physical fitting result (see Fig. 5a). The result is likely caused by the very fine microstructure of the high performance cement pastes (e.g., Paste2) and concretes

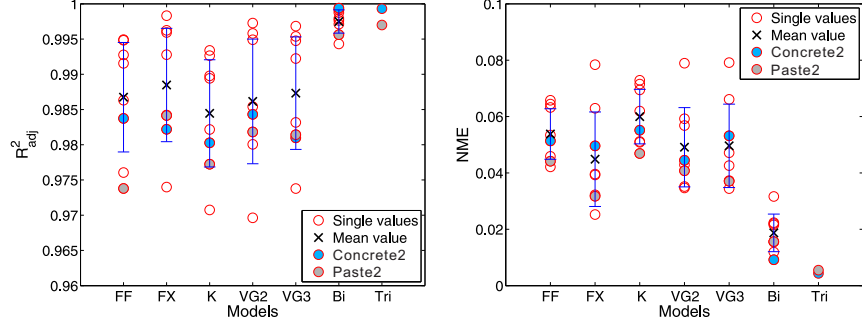


FIGURE 3: Comparison of  $R^2_{adj}$  and NME for desorption isotherms. Each circle ( $\circ$ ) in the figure stands for one material (see Table 2). Materials Concrete2 and Paste2 are highlighted. The error bars represent the standard deviation for each studied statistical criteria ( $R^2_{adj}$  and NME) and each model.

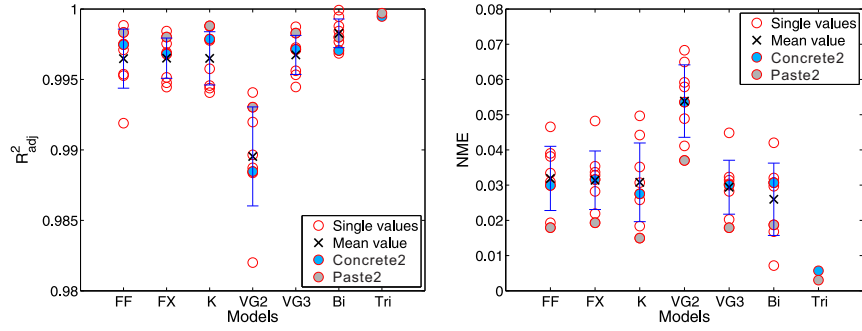


FIGURE 4: Comparison of  $R^2_{adj}$  and NME for adsorption isotherms. Each circle ( $\circ$ ) in the figure stands for one material (see Table 2). Materials Concrete2 and Paste2 are highlighted. The error bars represent the standard deviation for each studied statistical criteria ( $R^2_{adj}$  and NME) and each model.

(e.g., Concrete2). Because those materials can hold much water in the low RH range, the measured points in the low RH range are higher compared to the ordinary materials, such as the point at RH=12% in Fig. 5. This leads the non-physical fitting. Thus, it is worth fitting WVSIs by using higher modal models.

A comparison of uni-, bi- and tri-modal models is made in Fig. 5. The performance of the tri-modal model, nearly passing through all measured points, is obviously better than the uni- and the bi-modal models for both main isotherms in the low RH range. In terms of statistical analysis, using a tri-modal model improves the fitting results greatly (see highlighted values of  $R^2_{adj}$  and NME for Concrete2 and Paste2 in Figs. 3 and 4). In the high RH range, the tri-modal model yields the similar shape of curve to the bi-modal model.

However, the number of parameters in multi-modal models may be several times higher than in uni-modal models. This results in a more difficult fitting procedure and can even lead to instability. However, uni-modal models show acceptable fitting results for the selected database, except for high performance materials. The choice of WVSI model is thus highly dependent on the complexity of the measured isotherm.

Above, some commonly used WVSIs models have been compared to measured isotherms. In many cases, these models do not have a clear physical meaning. The models proposed by Fredlund and Xing [42], van Genuchten [38] and Brutsaert [45] originally came from Brooks and Corey's power type function [46], in which two parameters are involved, the air-entry pressure and a dimensionless parameter referring to the pore-size distribution [46]. When van Genuchten developed the closed form equation, the introduced parameter  $a_V$  was disconnected to the air-entry pressure [47]; the same is true for  $a_X$  in the FX model. So,  $a_V$  and  $a_X$  should be only seen as the air-entry pressure related parameter. In the same way,  $n_V$ ,  $m_V$ ,  $n_X$  and  $m_X$  are parameters related to the pore size distribution. The Kosugi's model [37] was developed for the soil and two parameters ( $P_{cm}$  and  $\sigma$ ) have to be determined based on the measured

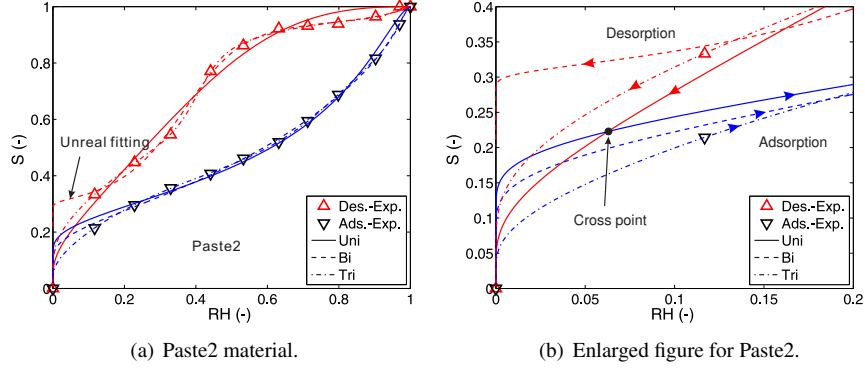


FIGURE 5: Fitting results for Paste2 material to compare results of uni-(VG2), bi- and tri-modal models. Fitting results for low RH values are shown in enlarged figures.

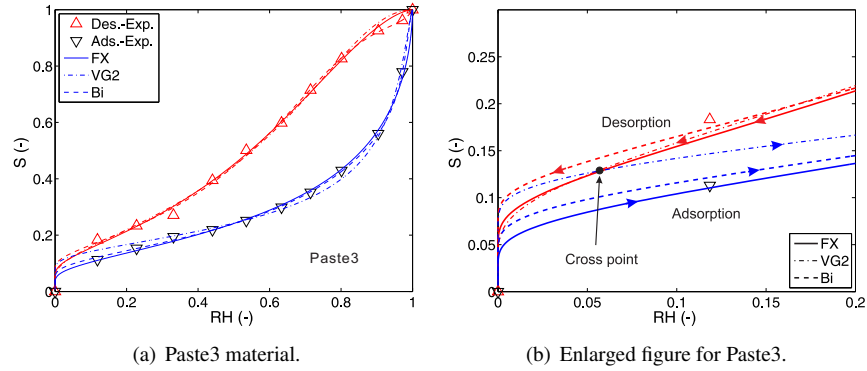


FIGURE 6: Fitting results for Paste3 material. To make the display clearly, only three models, VG2, FX and bi-modal models, are chosen to represent uni- and multi-modal models. Fitting results for low RH values are shown in the enlarged figure.

pore size distribution. Due to the lack of the experimental data of the pore size distribution for cementitious materials, the fitted  $P_{cm}$  and  $\sigma$  in this model cannot be verified whether they still retain the same physical meaning as when they were first introduced. The FF model is a pure empirical equation for the purpose of fitting the experimental data, without any physical meaning being mentioned.

To conclude the above comparisons, this paper recommends that uni-modal models, FX and VG3, can be used as a first tentative fitting. If one does not get satisfying fitting results, multi-modal models can be used. In next sections of this paper, the FX model will be used to fit the main sorption isotherms because it shows a slightly better performance to fit desorption isotherms than the VG3 model (see Fig. 3).

## 5. Prediction of one main isotherm from the other main branch

Most hysteresis models require at least both main curves to predict scanning loops. Nonetheless, measuring both sorption isotherms for cementitious materials is time consuming and quite costly. In practice, it is still under debate whether the initial fully dried state will change the microstructure during measurements of absorption isotherms. Instead, the desorption isotherm is easier to determine from an initially saturated state, which is also closer to the condition after the concrete structure formworks are removed. From this point of view, only the models to predict the adsorption isotherm from the desorption isotherm are evaluated herein.

In the literature, some comparisons have been done for sands and soils. Pham *et al.* [11] compared and ranked five selected models. Feng and Fredlund's model [41] (improved by Pham *et al.* [44]) appeared to be the most accurate one,

followed by Mualem Model IV [48]. Meanwhile, in Maqsoud's comparison [12], Parlange's model [49] (modified by Braddock *et al.* [50]) showed the best prediction for silty sand and fine sand.

According to the requirements of experimental data, comparisons will here be carried out in two groups : models only based on the measured main desorption branch and models needing additional data besides the main desorption branch.

### 5.1. Models only based on the measured main desorption branch

#### 5.1.1. Mualem Model II-1 [51]

The Mualem Model II-1 [51] is the extension of Mualem Model II [23]. In a totally homogeneous porous medium, two pore water distribution functions  $h$  and  $l$  can be considered identical for pore necks and pore bodies. This leads to  $h(\bar{\rho}) = l(\bar{\rho})$  (or  $h(\bar{r}) = l(\bar{r})$ ). Hence, the same distribution function is applied to both pore necks and pore bodies. The water distribution function (see Eq. 1) can be rewritten as :

$$f(\bar{r}, \bar{\rho}) = h(\bar{r})h(\bar{\rho}) \quad (18)$$

The water content during the wetting process (see Eq. 4) is rewritten as :

$$\theta_w(P_c) = \theta^{\max} H(P_c) \quad (19)$$

This simplification does not affect the expression for water content during a drying process (see Eq. 5). Combining Eq. (19) with Eq. (6), an equation calculating  $\theta_w(P_c)$  from  $\theta_d(P_c)$  is derived as :

$$\theta_w(P_c) = \theta^{\max} - [(\theta^{\max})^2 - \theta^{\max} \theta_d(P_c)]^{1/2} \quad (20)$$

The equivalent equation as a function of  $S$  is :

$$S_w(P_c) = 1 - [1 - S_d(P_c)]^{1/2} \quad (21)$$

#### 5.1.2. Parlange's model [49], modified by Braddock *et al.* [50]

Based on the Parlange's hysteresis model [49], an expression of the adsorption isotherm can be obtained as the following form.

$$\frac{dS_w}{dP_c} = \frac{S_w - S_d}{P_c} \quad (22)$$

Taking VG2 equation to describe the desorption isotherm and integrating Eq. (22), an analytical form of the adsorption isotherm was provided by Braddock *et al.* [50].

$$S_w = -\frac{P_c}{a_{dV}} + \left[ 1 + \left( \frac{P_c}{a_{dV}} \right)^{n_{dV}} \right]^{1/n_{dV}} \quad (23)$$

where  $a_{dV}$  and  $n_{dV}$  are fitting parameters for the desorption isotherm.

### 5.2. Models needing additional data besides the main desorption branch

#### 5.2.1. Feng and Fredlund's model [41], improved by Pham *et al.* [44]

From section 4, one may know that there are two coefficients in FF model [41] (see Eq. (12)). This indicates that two points on the adsorption isotherm are enough to determine these two parameters and to calculate the entire adsorption isotherm. Based on this idea, Pham *et al.* [44] introduced a method to find the positions of two such points (denoted by A and B). The position of point A corresponds to a capillary pressure :

$$P_{c,wA} = \left( \frac{a_d}{10} \right)^{1/b_d} \quad (24)$$

where  $a_d$  and  $b_d$  are parameters used in FF equation [41] for the desorption isotherm.

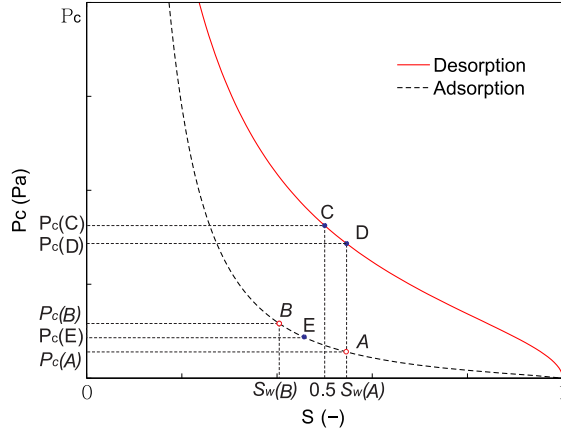


FIGURE 7: Schematic drawing of Feng and Fredlund's model [41] (improved by Pham *et al.* [44]) used to predict the adsorption branch from the desorption branch. Three points A, D and C are used to calculate point B.

Point B on the adsorption isotherm is defined as the point having a capillary pressure that is symmetrical to the capillary pressure of point A with respect to a horizontal line passing through point E on the adsorption isotherm (see Fig. 7).

$$|P_{c,wA} - P_{c,wE}| = |P_{c,wB} - P_{c,wE}| \quad (25)$$

In the above equation, the position of point E is unknown. Pham *et al.* [44] introduced a method to determine the position of point E. The authors defined two other points on the desorption isotherm to find point B. One point (C) is in the middle of the desorption isotherm (at  $S = 0.5$ ) :

$$P_{c,dC} = (a_d)^{1/b_d} \quad (26)$$

The other point (D) is on the desorption isotherm and has the same saturation value as point A :

$$P_{c,dD} = \left( \frac{a_d}{S_{wA}} - 1 \right)^{1/b_d} \quad (27)$$

Points A, C, D and E should satisfy the relation :

$$|P_{c,wA} - P_{c,wE}| = |P_{c,dD} - P_{c,dC}| \quad (28)$$

The capillary pressure of point B on the adsorption isotherm is obtained by solving Eqs. (25)-(28).

$$P_{c,wB} = P_{c,wA} - 2 \left[ \left( \frac{a_d}{S_{wA}} - a_d \right)^{1/b_d} - a_d^{1/b_d} \right] \quad (29)$$

Finally, the two parameters ( $a_w$  and  $b_w$ ) used in Feng and Fredlund's model [41] are calculated on the basis of the capillary pressures at points A and B.

$$a_w = \frac{S_{wA} P_{c,wA}^{b_w}}{1 - S_{wA}} \quad (30)$$

$$b_w = \frac{\log \left[ \frac{1 - S_{wB}}{S_{wB}} \frac{S_{wA}}{1 - S_{wA}} \right]}{\log \left[ \frac{P_{c,wB}}{P_{c,wA}} \right]} \quad (31)$$

### 5.2.2. Mualem Model IV [48]

The Mualem Model IV [48] is an improved version of Mualem Model II [23, 51]. In addition to the main desorption branch, a wetting scanning curve is needed to predict the main adsorption branch. The prediction is divided into two parts : from the highest capillary pressure to the starting point of the wetting scanning curve, and for capillary pressure lower than the starting point of the wetting scanning curve. The first part is predicted using the same method as Mualem Model II-1 [51]. The second part is calculated by using both the main desorption branch and the wetting scanning curve. Thus, for the main adsorption branch, the saturation can be expressed as follows :

$$S_w(P_c) = \begin{cases} 1 - [1 - S_d(P_c)]^{1/2} & \text{for } P_{c,1} \leq P_c \leq P_c^{\max} \\ 1 - \frac{1 - S_{l,w}(P_c)}{[1 - S_d(P_{c,1})]^{1/2}} & \text{for } P_c^{\min} \leq P_c < P_{c,1} \end{cases} \quad (32)$$

where  $P_{c,1}$  is the capillary pressure at the starting point of the additional wetting scanning curve. The subscript  $(l,w)$  represents the first wetting scanning curve.

The accuracy of this model is sensitive to the position of the starting point of the wetting scanning curve. If the scanning curve starts at a high RH, the model tends to be the same as Mualem Model II-1 [51]. If the scanning curve starts at a low RH, it will only use the wetting scanning curve to predict the adsorption isotherm. According to the position of the starting point in available experimental data, comparisons were performed in three levels : low RH ( $RH_1 = 12\%$ ), medium RH ( $RH_1 = 33\%$ ) and high RH ( $RH_1 = 53\%$ ). Not all materials in the database can reach this requirement. Only five materials (Concrete1, Concrete2, Concrete3, Paste2 and Paste3) are used for validation and comparisons.

### 5.3. Comparison of results and discussion

The prediction results of Paste2 are shown in Figs. 8 (other comparison results are included in the document “supplementary materials”). For the models only using the main desorption curve (Mualem Model II-1 [51] and Parlange’s model [49] modified by Braddock *et al.* [50]), the standard deviation of the statistical criteria  $R_{adj}^2$  and NME are very large (see Fig. 9). Furthermore,  $R_{adj}^2$  values are low and NME values are high. Figure 8 also displays that the prediction of these two models do not show good agreements with measured curves. As a result, one can conclude that only using one main curve is not sufficient to predict the other main curve in the case of cementitious materials.

With regard to models needing additional data, Fig. 9 clearly shows that the improved Feng and Fredlund’s model [41] yields the best prediction with the highest  $R_{adj}^2$  and the lowest NME. This is due to the fact that adding two additional measured points significantly improves the prediction accuracy. In spite of needing one wetting scanning curve, by contrast, Mualem Model IV [48] does not provide good performance, regardless of the level of RH.

The requirement of additional experimental data limits the application of the improved Feng and Fredlund’s model [41]. In fact, the positions of points A and B depend on the shape of the desorption isotherm ; thus, they vary according to the studied materials. If these two points are fixed independently of the material, it will be more interesting from a practical point of view to determine the adsorption isotherm. The mean RH values for these two points are calculated according to the prediction results, which are around 67% and 86%. They almost correspond to the RH values (63.2% and 90.4%) used in the measurements of the sorption isotherms in [5]. Thus, these two points can be fixed at 63.2% and 90.4%. The main adsorption isotherms can be determined by using Eq. (12). The predicted results are compared with other methods in Fig. 9. It is clear that the fixed points method has the equivalent accuracy as Feng and Fredlund’s model [41] (improved by Pham *et al.* [44]). This implies that if one wants to know the entire adsorption isotherm, it is enough to determine two adsorption points at  $RH = 63.2\%$  and  $90.4\%$ .

The above comparisons reveal that it may be not appropriate to predict one main isotherm by using the other main isotherm only (*e.g.*, Mualem Model II-1 [51] and Parlange’s model [49] modified by Braddock *et al.* [50]). Two additional measured points on the adsorption isotherm can provide a better prediction (improved Feng and Fredlund model [41]) than using one wetting scanning curve (Mualem Model IV [48]).

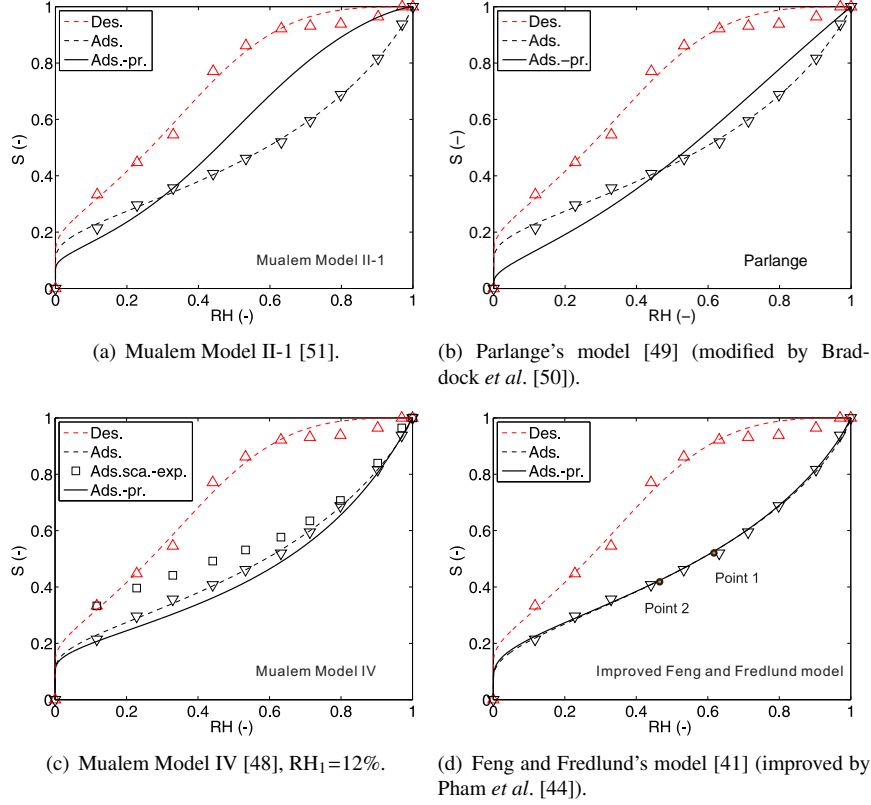


FIGURE 8: Prediction results for Paste2 material. Two points in the Feng and Fredlund's model [41] (improved by Pham *et al.* [44]) are at RH = 67% and RH = 46%.

## 6. Prediction of scanning isotherms

Comparisons of different hysteresis models can be found in the literature [11, 30, 52–54] for a large variety of porous media, not including cementitious materials. By statistical analysis, Viaene *et al.* [52] concluded that models developed based on domain theories give the best predictions. A similar conclusion has been drawn in the comparisons performed by Pham *et al.* [11]. However, besides the domain models, several recently developed empirical models were also selected for comparisons due to their simplicity of application.

### 6.1. Mualem Model II [23]

In Mualem Model II [23], a series of equations to calculate scanning curves have been proposed based on Mualem's diagram (see Fig. 2). They use two basic functions  $H$  (see Eq. 3) and  $L$  (see Eq. 6), which are determined by two main sorption isotherms (desorption and adsorption). Rewriting them as a function of  $S$ , we get :

$$L(P_c) = S_w(P_c) \quad H(P_c) = \frac{S_d(P_c) - S_w(P_c)}{1 - S_w(P_c)} \quad (33)$$

The first scanning curve in drying (scanning curve of order  $N = 1$ ), starting on the adsorption isotherm at the point  $(S_w(P_{c,1}), P_{c,1})$ , is formulated according to Mualem's diagram :

$$S_{1,d}(P_c) = S_w(P_{c,1}) - [L(P_{c,1}) - L(P_c)][1 - H(P_c)] \quad (34)$$

The first scanning curve in wetting (order  $N = 1$ ), starting on the desorption isotherm at the point  $(S_d(P_{c,1}), P_{c,1})$ , is calculated by :

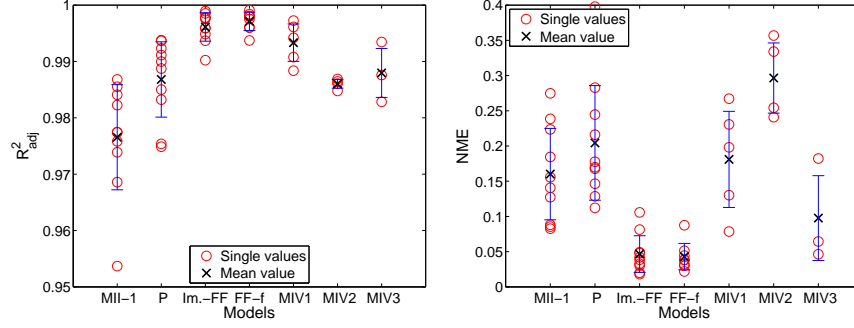


FIGURE 9: Comparison results of predicting the main adsorption branch from the main desorption branch. Results are from models : Mualem Model II-1 (MII-1) [51], Parlange's model (P) [49] (modified by Braddock *et al.* [50]), Feng and Fredlund model's (FF) [41] (improved by Pham *et al.* [44]), fixed points version of Feng and Fredlund's model (FF-f) and Mualem Model IV [48] of the wetting scanning curve starting at  $RH_1=12\%$  (MIV1),  $RH_1=33\%$  (MIV2) and  $RH_1=53\%$  (MIV3).

$$S_{1,w}(P_c) = S_d(P_{c,1}) + [L(P_c) - L(P_{c,1})] H(P_{c,1}) \quad (35)$$

It can be noted that the expression for the first drying scanning is different to the first wetting scanning curve. The expression for the wetting scanning curve of order  $N$  (odd number and  $> 1$ ) is deduced according to Mualem's diagram :

$$S_{N,w}(P_c) = S(P_{c,N}) + [L(P_c) - L(P_{c,N})] [1 - H(P_{c,N})] \quad \text{for } L(P_c) \leq L(P_{c,N-1}) \quad (36)$$

where  $S(P_{c,N})$  is the saturation at the starting point of the current scanning curve, which must be the end point of the previous scanning curve. If  $L(P_c) \geq L(P_{c,N-1})$ , Mualem's diagram indicates that  $L(P_{c,N-3})$  will be used instead of  $L(P_{c,N-1})$  until the scanning curve reduces to the main isotherms (order  $N = 0$ ). For example, in Fig. 10, if the third scanning curve in wetting CB continues to decrease after point B, it must do so on curve BD, which is the extension line of the first scanning curve in wetting AB. This ensures that all scanning loops are closed and enclosed in the main loop.

In the same manner, the expression for the drying scanning curve of order  $N$  (even number) is written as :

$$S_{N,d}(P_c) = S(P_{c,N}) - [L(P_{c,N}) - L(P_c)] [1 - H(P_c)] \quad \text{for } L(P_c) \geq L(P_{c,N-1}) \quad (37)$$

If  $L(P_c) \leq L(P_{c,N-1})$ ,  $L(P_{c,N-3})$  will be used instead of  $L(P_{c,N-1})$  for calculation.

Equations (35-37) comprise a set of formulas to calculate arbitrary scanning loops.

## 6.2. Mualem dependent model [25–27]

Based on the assumption of *dependent* of the neighbouring pores in Mualem Model III [25], Mualem and Miller [26] and Mualem [27] have provided different weighting functions  $p_d$  to improve the prediction of the scanning curves. The improved version in [27] seems to provide a better agreement with the experimental data for soils [27, 28, 54]. This version (hereafter called *Mualem dependent model*), as the same as Mualem Model II [23], only needs both main sorption isotherms. The formula of  $p_d$  is given as [27] :

$$p_d(S) = \frac{1 - S}{[1 - S_w(P_c^+)]^2} \quad (38)$$

where  $P_c^+$  is the capillary pressure at  $S_d(P_c^+) = S$  (the current saturation, see Fig. 11).

The function for the first scanning curve in drying (order  $N = 1$ ), starting on the adsorption isotherm, is deduced as :

$$S_{1,d}(P_c) = S_w(P_{c,1}) - p_d(S) [1 - S_w(P_c)] [S_w(P_{c,1}) - S_w(P_c)] \quad (39)$$

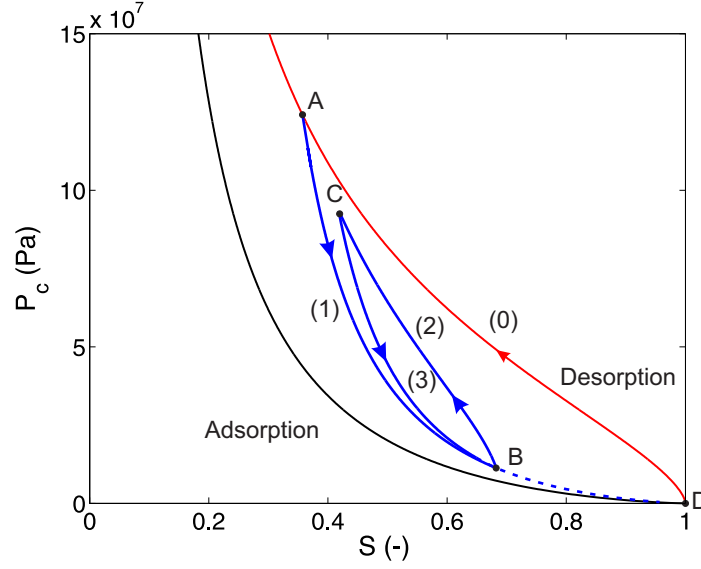


FIGURE 10: An example of scanning loops calculated by Eqs. (35)-(37).

The first scanning curve in wetting (order  $N = 1$ ), starting on the main desorption isotherm, can be calculated by :

$$S_{1,w}(P_c) = S_d(P_{c,1}) + p_d(S_1) [1 - S_w(P_{c,1})] [S_w(P_c) - S_w(P_{c,1})] \quad (40)$$

where  $p_d(S_1)$  is  $p_d$  at the starting point  $(S_d(P_{c,1}), P_{c,1})$ . Functions for scanning loops can be easily derived based on Mualem's diagram [25–27]. For the wetting scanning curves of order  $N$  (odd number and  $> 1$ ), the expression is written as :

$$S_{N,w}(P_c) = S(P_{c,N}) + p_d(S_N) [1 - S_w(P_{c,N})] [S_w(P_c) - S_w(P_{c,N})], S_w(P_c) \leq S_w(P_{c,N-1}) \quad (41)$$

For the drying scanning curves of order  $N$  (even number), the expression is :

$$S_{N,d}(P_c) = S(P_{c,N}) - p_d(S) [1 - S_w(P_c)] [S_w(P_{c,N}) - S_w(P_c)], S_w(P_c) \geq S_w(P_{c,N-1}) \quad (42)$$

One can see that wetting scanning curves are provided by explicit formulas, while equations for drying scanning curves are implicit forms with respect to the current capillary pressure  $P_c$ . Therefore, a drying scanning curve must be calculated by an iterative method. Substitution of Eq. (38) into Eq. (40) yields the same equation for the first scanning curve in wetting as the one used by Mualem Model II. It means that these two models will share the same first wetting scanning curve.

### 6.3. Incremental models

Elastoplastic models have been used in porous media field to describe the relation between  $P_c$  and  $S$  [32, 33]. Usually, a simple incremental relation is used. It is generally assumed that the differential of  $P_c$  on the scanning curve is related to the differential of  $P_c$  or  $S$  on the main isotherm. Two typical models are described below.

#### (1) Li's model [32]

In this method, the scanning curve is obtained by integrating the incremental relation  $dP_c - dS$ . A proposition for the incremental form of  $P_c(S)$  is given in [32] as follows :

$$d \ln[P_c(S)] = \left[ \frac{\ln[\bar{P}_c(S)] - \ln(P_{c,1})}{\ln[P_c(S)] - \ln(P_{c,1})} \right]^\beta d \ln[\bar{P}_c(S)] \quad (43)$$

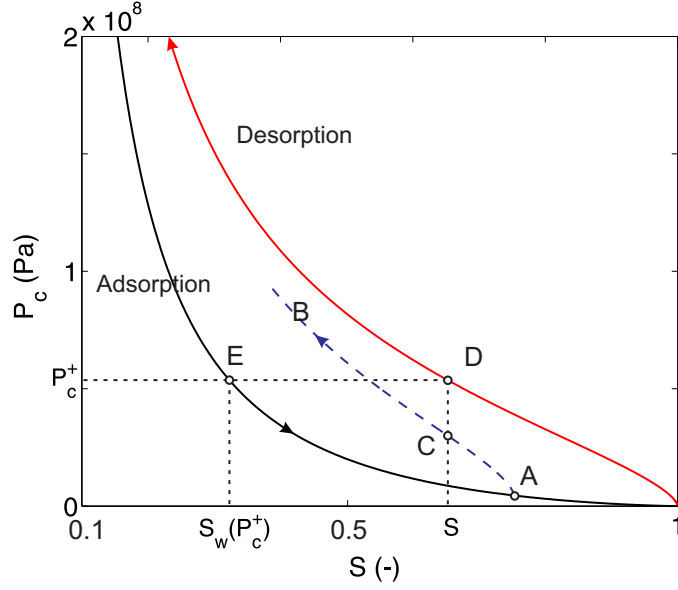


FIGURE 11: The calculation of  $p_d$  during a drying process in Mualem dependent model [27].

where  $\beta$  is a material parameter.  $\bar{P}_c(S) = P_{c,d}(S)$  is the capillary pressure on the main desorption branch for the drying process and  $\bar{P}_c(S) = P_{c,w}(S)$  is on the main adsorption branch for the wetting process. By integrating Eq. (43), one can obtain the expressions for a drying scanning curve,

$$\ln[P_c(S)] = \ln(P_{c,1}) + \left( |\ln[P_{c,d}(S)] - \ln(P_{c,1})|^{\beta_d+1} - |\ln(P_{c,d1}) - \ln(P_{c,1})|^{\beta_d+1} \right)^{1/(\beta_d+1)} \quad (44)$$

and for a wetting scanning curve,

$$\ln[P_c(S)] = \ln(P_{c,1}) - \left( |\ln(P_{c,1}) - \ln[P_{c,w}(S)]|^{\beta_w+1} - |\ln(P_{c,1}) - \ln(P_{c,w1})|^{\beta_w+1} \right)^{1/(\beta_w+1)} \quad (45)$$

One can notice that in this method the scanning curve always starts with an infinite slope (*i.e.*,  $|dP_c/dS| \rightarrow \infty$ ).

(2) *Wei's model* [33]

Based on reference [55], Wei *et al.* [33] suggested a new and simpler incremental relation, expressed as :

$$dP_c = -K_p dS \quad (46)$$

where  $-K_p$  is the slope of the scanning curve.

According to Wei's theory, when  $P_c$  changes, the water content in the material is assumed to be additively decomposed into two parts, a reversible part and an irreversible part. The irreversible part of water content is dependent on the capillary pressure, while the reversible part is independent. Accordingly, the slope of each scanning curve can be divided into two parts, one is an irreversible part affected by the main isotherm (*e.g.*, the first term on the right side of Eq. 47), and the other is based on the effect of both reversible and irreversible water content (*e.g.*, the second term on the right side of Eq. 47). At current  $P_c$ , the slope of the drying scanning curve could be calculated by :

$$K_p = -\frac{dP_{c,d}(S)}{dS} + \frac{c_d|P_c - P_{c,d}(S)|}{P_{c,d}(S) - P_{c,w}(S) - |P_c - P_{c,d}(S)|} \quad (47)$$

For a wetting scanning curve, it is :

$$K_p = -\frac{dP_{c,w}(S)}{dS} + \frac{c_w|P_c - P_{c,w}(S)|}{P_{c,d}(S) - P_{c,w}(S) - |P_c - P_{c,w}(S)|} \quad (48)$$

where  $c_d$  and  $c_w$  are the internal state variables for drying and wetting processes, respectively. In Eqs. (47) and (48), the slope of the main sorption isotherm ( $-\frac{dP_{c,d}(S)}{dS}$ ) and the distance between two main isotherms ( $P_{c,d}(S) - P_{c,w}(S)$ ) represent irreversible effects. The part of  $|P_c - P_{c,d}(S)|$ , depending on the current capillary pressure, represents the reversible effect. The coefficients of  $c_d$  (or  $c_w$ ) is used to control the reversible effect and it is a function of the water content. To simplify the application of this model, Wei *et al.* [33] assumed constant values of  $c_d$  and  $c_w$ . Clearly, the reversible effect can be observed at the beginning of the scanning curve due to the large initial slope, like it has been illustrated by Wei *et al.* [33] and in the model of Hogarth *et al.* [56, 57] for soils.

When Eqs. (47) and (48) are applied to simulate scanning curves for cementitious materials, the model predict that the scanning curve crosses the main sorption isotherm because of the significant reversible effect. However, experimental data of the scanning curves [5, 36] do not show such a reversible effect. Hence, a modification to Eqs. (47) and (48) is proposed in the present paper to reduce the reversible effect and new relations are yielded for a drying scanning curve :

$$K_p = -\frac{dP_{c,d}(S)}{dS} + \frac{c_d|P_c - P_{c,d}(S)|}{P_{c,d}(S) - P_{c,w}(S)} \quad (49)$$

and for a wetting scanning curve.

$$K_p = -\frac{dP_{c,w}(S)}{dS} + \frac{c_w|P_c - P_{c,w}(S)|}{P_{c,d}(S) - P_{c,w}(S)} \quad (50)$$

One can notice that  $K_p$  depends on the current position of the scanning curve. An iterative method is needed to compute the current capillary pressure.

#### 6.4. Improved Rubin's empirical hysteresis model [58]

The basic idea for the calculation of the scanning curve is to determine the distance between the scanning curve and the main isotherm which the scanning curve approaches. Here, considering the saturation as an independent variable, the present paper takes the prediction of the drying scanning curve as an example of how to develop an empirical hysteresis model.

As above models show, the distance between the drying scanning curve and the main desorption curve should be a function of the current saturation ( $S_d$ ) and the starting point of the scanning curve, which is simply formulated as :

$$P_{c,d} - P_c = F(S_d, P_{c,1}, S_1) \quad (51)$$

Various  $F$  functions can be found in the literature. For instance, Rubin [58], as well as Feng and Fredlund [41], proposed expressions for the first drying scanning curve, considering  $F$  as proportional to the distance between the two main isotherms. Nevertheless, these two models did not take into account the position of the starting point in their expressions. Thus, these expressions were only valid for the first scanning curve in drying and not able to simulate scanning loops. Here, a new  $F$  is introduced by adapting the original form in [58]. The exponential relation is used to control how fast the scanning curve approaching the main isotherm. Finally, the following expression is given for the drying scanning curve :

$$P_c(S) = P_{c,d}(S) - [P_{c,d}(S) - P_c(S_1)] \exp[\gamma_d(S - S_1)] \quad (52)$$

The negative value of  $\gamma_d(S - S_1)$  limits the exponential expression from 1 (at the starting point) to near 0 (almost on the main isotherm). Similarly, the expression for the wetting scanning curve is derived as :

$$P_c(S) = P_{c,w}(S) + [P_c(S_1) - P_{c,w}(S)] \exp[\gamma_w(S_1 - S)] \quad (53)$$

The constant  $\gamma_d$  and  $\gamma_w$  are used to determine the shape of the scanning curve and needs to be assessed from experimental data.

## 6.5. Comparison of results and analysis of hysteresis models

### 6.5.1. Predictions of the first scanning curves

Overall, five materials, Concrete1, Concrete2, Concrete3, Paste2 and Paste3 (see Table 2), have been studied. One example of a comparison between experimental data and predictions (Paste3) performed by above models are provided in Fig. 12 (other comparison results are included in the document “supplementary materials”). The results obtained by Mualem Model II [23] and Mualem dependent model [27] are illustrated in the same figure. For the empirical models with unknown parameters ( $\beta_d$  and  $\beta_w$  in Eqs. 44 and 45,  $c_d$  and  $c_w$  in Eqs. 49 and 50 and  $\gamma_d$  and  $\gamma_w$  in Eqs. 52 and 53), the models have been optimized to predict all measured wetting scanning curves for each material.

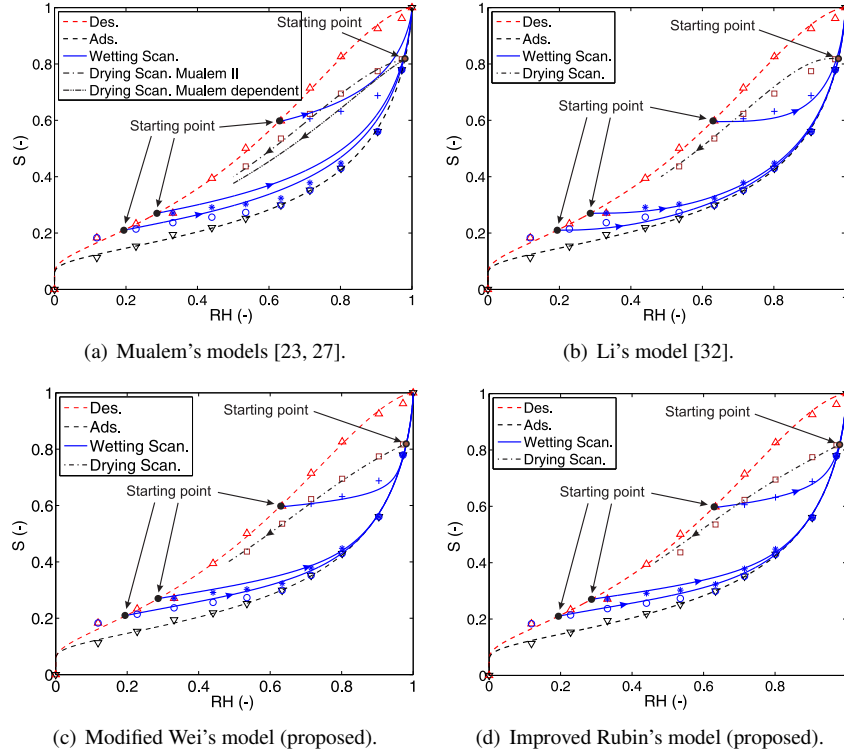


FIGURE 12: Predicted wetting scanning curves (solid lines) and drying scanning curves (dashed-dotted lines) for Paste3 compared with experimental data (symbols) from [5].

The empirical models reveal that the predicted wetting scanning curves increase slowly at the beginning where the curves are almost parallel to the horizontal axis (see Fig. 12), so that these curves can approach the main adsorption branch quickly. This has been observed by Åhs [36] in experimental results on the hardened cementitious materials. As a consequence, the first wetting scanning curves probably reach the main curve before  $RH = 100\%$ , as illustrated by modified Wei's model and improved Rubin's model (see Fig. 12). The wetting scanning curves predicted by Mualem's models [23, 27] increase more smoothly and reach the main wetting curve at  $RH$  close to  $100\%$ . This results in a poorer agreement with measured data than empirical models.

Experimental data for the first drying scanning curves are only available for Paste2 and Paste3 materials in our database [5]. Predictions from Mualem Model II [23] show that curves decrease with a lower slope and turn towards the desorption isotherm more gently than curves predicted by the empirical models. Therefore, the empirical models yield predictions with a lower accuracy compared with Mualem Model II. With respect to Mualem dependent model [27], it does not provide a good prediction for the drying scanning curves (see Fig. 12a).

The two criteria  $R^2_{adj}$  and NME for the prediction of the first wetting scanning curves are shown in Fig. 13. They illustrate that the empirical models can give higher  $R^2_{adj}$  and lower NME values than the Mualem Model II. This is definitely due to that the two additional parameters in the empirical models can be adjusted to fit the experimental

data, while Mualem's models essentially depend on the shape of the two main sorption isotherms. In contrast, in the prediction of the first drying scanning curves for Paste3, Mualem Model II reveals better prediction than the empirical models.

Figure 13 also shows that all empirical models have almost equal accuracy for the estimation of the first scanning curves, either wetting or drying. None of the selected hysteresis models is considerably better than the others. This conclusion is similar to that reported by Jaynes [30] when he compared hysteresis models for soils. Hence, it needs the comparison of higher order scanning curves.

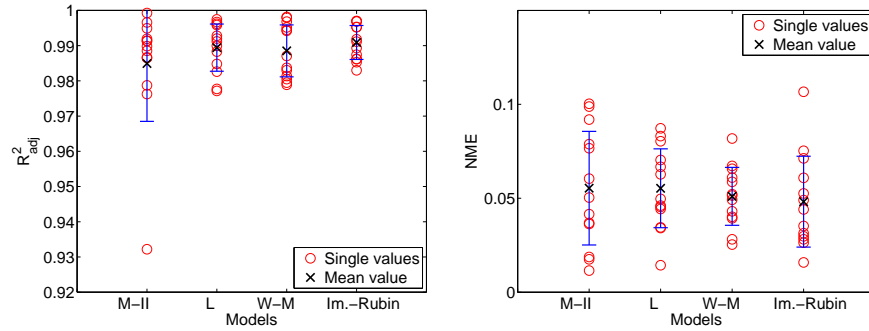


FIGURE 13: Comparison results for wetting scanning isotherm predicted by Mualem Model II (M-II) [23], Li's model (L) [32], modified Wei's model (W-M) [33] and improved Rubin's model (Im.-Rubin) [58].

### 6.5.2. Predictions of scanning loops

Scanning loops have been measured for Paste2 and Paste3 [5]. Here three measured loops, one for Paste2 and two for Paste3, have been chosen to verify the applicabilities of the selected hysteresis models. One of the prediction result is shown in Fig. 14 (other comparison results are included in the document "supplementary materials").

Because of the poor prediction of the first wetting scanning curves, Mualem dependent model [27] do not show better prediction results than Mualem Model II [23]. Among the empirical models, Li's model [32] appears to be the best one to predict the shape of the measured scanning loops. Besides, the improved Rubin's model [58] shows a better prediction of secondary drying scanning curves than the modified Wei's model [33] (see Fig. 14).

### 6.5.3. Analysis of the pumping effect

One hysteretic behavior, called the *pumping effect*, should be noticed for the empirical models. It refers to the non-closure of scanning loops when the secondary and higher order scanning curves are calculated. Researchers consider that the pumping effect is an artifact of the algorithm and does not correspond to an actual material property [57, 59]. Thus, this behavior is also called the *pumping errors* (PEs), which is defined and illustrated in Fig. 15. Point A is the starting point of the scanning loop. Point B is on the secondary scanning curve in drying at the same RH as point A. The difference of  $S$  between A and B is defined as the *drying pumping error* (DPE). Similarly, a *wetting pumping error* (WPE), originating from wetting scanning curves (difference between point C and point D in Fig. 15), is also observed for the empirical models. Figure 15 implies the amplitudes of DPE and WPE can be quantified.

The evolution of PE is not only dependent upon the initial state but also upon the magnitude of the RH oscillations. Thus, to assess the evolution of DPE and WPE, two initial states of RH cycles are tested : an initial drying state and an initial wetting state. Paste3 material is taken as an example because many measured scanning curves are available for this material, including the first and secondary drying curves and the first wetting scanning curves. Two RH oscillations have been chosen for each initial state. The first one has been provided by experiments, with RH changing between 63% and 97%. The second one reduces the RH difference to 20%, such as for an RH oscillating between 63% and 83%.

The simulated results of PEs *vs.* the number of cycles are plotted in Fig. 16. The PEs are clearly more significant for the small RH oscillations than for the large RH oscillations. The first loop produces the largest PE, and then it reaches a constant value after about 2 cycles for the large RH oscillations and about 5 cycles for the small RH oscillations.

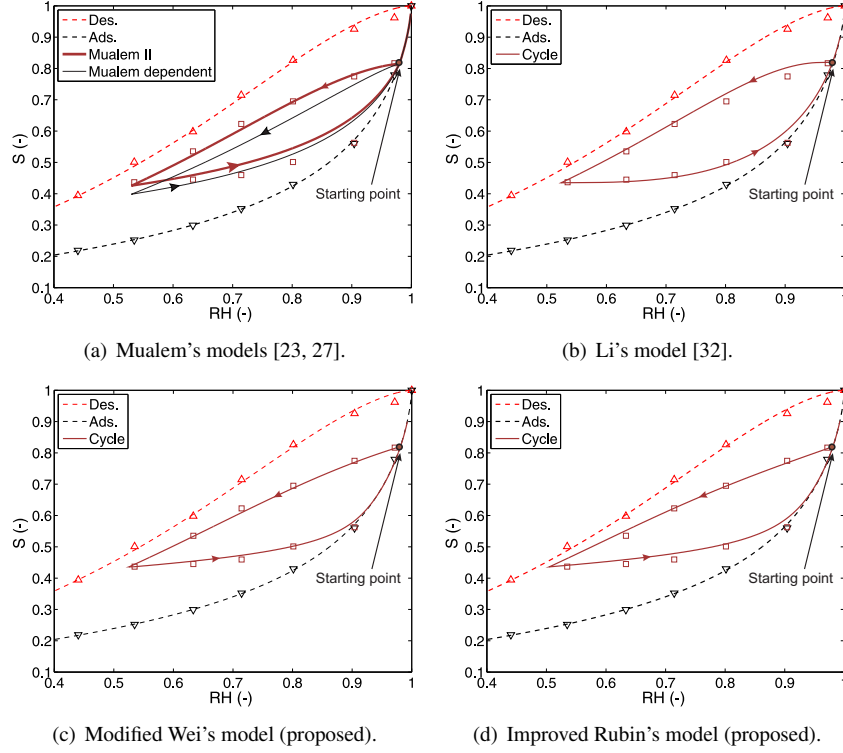


FIGURE 14: Predicted scanning loop (solid lines) for Paste3 compared with experimental data (symbols) from [5]. Simulated RH cycle : 97%  $\rightarrow$  53%  $\rightarrow$  99%.

Li's [32] and improved Rubin's models [58] provide similar PE (less than 0.1) for the large RH oscillations, while improved Rubin's model yields larger PE (around 0.3) than Li's model (around 0.2) for small RH oscillations. It is also clear that WPEs are larger than DPEs in both empirical models for the same kind of the RH oscillations.

For the large RH changes, PEs of the empirical models are acceptable. Nevertheless, for the small RH oscillations, if the model fails to eliminate PEs, the cumulative errors associated with oscillations of hysteresis loops are probably significant and lead to unrealistically simulated results. Some works have been done to avoid PEs when a hysteresis model was developed. By assuming that scanning curves have the same shape as the main branches, Parker and Lenhard [60] and Huang *et al.* [57] enforced closure of scanning loops to eliminate pumping errors. The problem of these methods is that they need to rescale and reformulate each scanning curve if the direction changes, and this may be inefficient for modelling of frequent drying and wetting cycles.

## 6.6. Discussion

Compared with the empirical models, Mualem's models (Model II [23] and dependent model [27]) have the advantage to avoid PE, even though their predictions are not as good as the empirical models. They may be more applicable for smaller RH oscillations comparing with the empirical models. Another advantage of Mualem's models is that they need only the two main sorption isotherms to predict scanning loops, unlike the empirical models that require at least two scanning curves to determine parameters.

Notably, from a practical point of view, equations of Mualem Model II [23], Li's model [32] and improved Rubin's model are expressed in explicit forms which are easier to implement in a numerical modelling of moisture transport. In particular, the improved Rubin's model uses very simple equations and provides an acceptable prediction. The modified Wei's model [33] and Mualem dependent model [27] correspond to implicit formulas which significantly increase the difficulty to apply them.

To conclude the above analysis about hysteresis models, this paper recommends Mualem Model II [23], Li's [32] and improved Rubin's models in the case of moisture transport modelling within cementitious materials exposed to

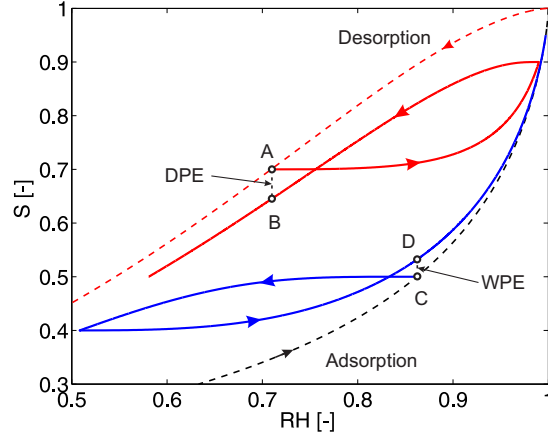


FIGURE 15: Definitions of DPE and WPE.

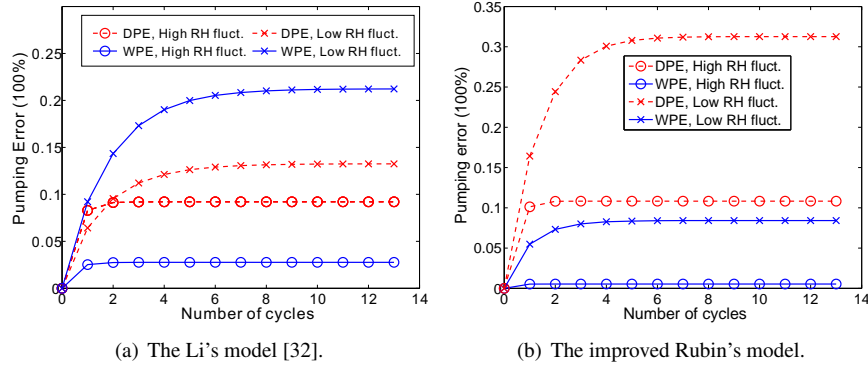


FIGURE 16: PE evolutions calculated based on two RH fluctuations.

cyclic boundary conditions. Two empirical models (Li's [32] and improved Rubin's models) are more suitable for large RH oscillations, in which pumping effects can be reduced.

## 7. Conclusions and recommendations

Detailed comparisons of hysteresis models for cementitious materials have been done in this study. Experimental results measured by the saturated salt solution method have been used for the validation and verification of models. Two statistical criteria  $R_{adj}^2$  and NME have been employed to evaluate models and their relevance. In regard to the proposed multi-level hysteresis modelling presented in Table 1, above studies indicate that Level 1 and Level 2 provide more reliable prediction results. Because there is no model that can predict one main curve well only on the basis of the other main curve, the prediction accuracy of Level 3 is not satisfactory. Evaluations for all selected models, the main features, disadvantages, and our recommendations, are summarised in the document "supplementary materials". Conclusions can be drawn from above comparisons.

1. Even though cementitious materials have quite different pore structures compared with soils and sands, most selected models in the present paper can provide a satisfactory fitting or prediction in the case of cementitious materials.
2. Concerning the fitting of the main branches, three-parameter fitting models provide better results than two-parameter models. That means if one wants to predict both main sorption isotherms, at least three points for each isotherm have to be measured.

3. The models selected for predicting one main isotherm from the other main isotherm are not satisfactory. However, by using two additional points on the adsorption isotherm, the Fend and Fredlund's model [41] (improved by Pham *et al.* [44]), shows a high prediction accuracy. In the present paper, it is found that if these two points are fixed at RH = 63.2% and 90.4%, the model still provides very good prediction. This result could be used to determine the main adsorption branch based on the experimental data at these two points.
4. Among the hysteresis models, the empirical ones provide better predictions but pumping errors cannot be avoided with these models. In contrast, Mualem's models show no pumping errors, but predictions do not agree with experimental data as well as the empirical models. It indicates two potential ways to develop a new hysteresis model : one is to improve the accuracy of the conceptual models ; the other way is to develop empirical models without pumping errors.

This study has investigated the use of hysteresis models to fit the main sorption isotherms and to predict the scanning loops. The purpose is to recommend hysteresis models for modelling of moisture transport in cementitious materials under cyclic drying and wetting conditions. In the future, the implementation of selected hysteresis models into moisture transport models will provide further comparisons with experimental data, such as water content profiles (*e.g.*, gamma-ray attenuation profiles and NMR profiles). Furthermore, these models will be coupled with the available ions transport models [61, 62] and to assess durability of concrete structures exposed to various environments.

## Acknowledgement

The research leading to these results has received funding from the European Union Seventh Framework Programme (FP7 / 2007-2013) under grant agreement 264448.

## Nomenclature

$\bar{\rho}$	Normalized radii of pore bodies	-
$\bar{P}_c(S)$	The capillary pressure on the main sorption isotherm used in the Li's model	Pa
$\bar{r}$	Normalized radii of pore necks	-
$\beta_d, \beta_w$	Parameters used in the Li's model	-
$\gamma_d, \gamma_w$	Parameters used in the improved Rubin's model	-
$\rho_l$	Liquid-water density	$\text{kg} \cdot \text{m}^{-3}$
$\sigma$	The standard deviation of log-transformed pore radius	-
$\theta$	Water content	$\text{m}^3 \cdot \text{m}^{-3}$
$\theta^{\max}$	The maximum water content	$\text{m}^3 \cdot \text{m}^{-3}$
$\theta_r$	Water content at dry reference state	$\text{m}^3 \cdot \text{m}^{-3}$
$a_F$	Parameters in the FF model	Pa
$a_F$	Parameters in the FX model	Pa
$a_V$	Parameters in the van Genuchten's model	Pa
$a_{dV}$	Parameters for desorption isotherm in the Parlange's model	Pa
$a_d$	Parameters for the main desorption branch in the Feng and Fredlund's model	Pa
$a_w$	Parameters for the main adsorption branch in the Feng and Fredlund's model	Pa
$b_F$	Parameters in the FF model	-

$b_d$	Parameters for the main desorption branch in the Feng and Fredlund's model	-
$b_w$	Parameters for the main adsorption branch in the Feng and Fredlund's model	-
$c_d, c_w$	Parameters used in the Wei's model	-
$f(\bar{r}, \bar{\rho})$	The total pore water distribution function	-
$h(\bar{r})$	The pore water distribution function related to pore necks	-
$H(P_c)$	The cumulative pore water distribution function related to pore necks	-
$K_p$	The slope of a scanning curve	-
$l(\bar{\rho})$	The pore water distribution function related to pore bodies	-
$L(P_c)$	The cumulative pore water distribution function related to pore bodies	-
$m$	The number of undetermined parameters in a model	-
$m_F, n_F$	Parameters in the FX model	-
$M_v$	The molar mass of water molecule	$\text{kg} \cdot \text{mol}^{-1}$
$m_V, n_V$	Parameters in the van Genuchten's model	-
$n$	The number of measured data	-
$n_{dV}$	Parameters for desorption isotherm in the Parlange's model	-
$P_c$	Capillary pressure	Pa
$p_d$	A weighting factor used for the drying process in Mualem dependent model	-
$p_w$	A weighting factor used for the wetting process in Mualem dependent model	-
$P_{c,1}$	Capillary pressure at the first point of a scanning curve	Pa
$P_{c,d1}$	Capillary pressure on the main desorption branch at the same saturation as the first point of a scanning curve	Pa
$P_{c,dA}$	Capillary pressure at point A on the main desorption branch	Pa
$P_{c,d}$	Capillary pressure of the main desorption branch	Pa
$P_{c,w1}$	Capillary pressure on the main adsorption branch at the same saturation as the first point of a scanning curve	Pa
$P_{c,wA}$	Capillary pressure at point A on the main adsorption branch	Pa
$P_{c,w}$	Capillary pressure of the main adsorption branch	Pa
$P_c^+$	The capillary pressure used to calculate $p_d(S)$ in the Mualem dependent model	Pa
$Q$	The complementary normal distribution function	-
$R$	The gas constant	$\text{J} \cdot \text{K}^{-1} \cdot \text{mol}^{-1}$
$R^2$	The coefficient of determination	-
$R_{adj}^2$	The adjusted $R^2$	-
$RH$	Relative humidity	-
$RH_1$	RH at the first point of a scanning curve	-
$S$	Saturation	-
$S(P_{c,N})$	Saturation at the starting point of the current scanning curve	-

$S_{1,d}(P_c)$	Saturation of the first scanning curve in drying	-
$S_{1,w}(P_c)$	Saturation of the first scanning curve in wetting	-
$S_1$	Saturation at the first point of a scanning curve	-
$S_d$	Saturation of the main desorption branch	-
$S_{N,d}(P_c)$	Saturation of the $N$ th scanning curve in drying	-
$S_{N,w}(P_c)$	Saturation of the $N$ th scanning curve in wetting	-
$S_w$	Saturation of the main adsorption branch	-
$T$	Temperature	K
$w_i$	weighting factor for pore system $i$ in the multi-modal model	-
$P_c^{\max}$	The maximum capillary pressure	Pa
$P_c^{\min}$	The minimum capillary pressure	Pa
$P_{cm}$	Capillary pressure related to the medium pore radius	Pa
NME	The normalized mean error	-
<b>Subscripts</b>		
$d$	Drying or desorption process	-
$w$	Wetting or adsorption process	-

## Appendix A. Supplementary materials

- [1] O. Coussy, Mechanics of porous continua, Wiley, New York, 1995.
- [2] R. M. Espinosa, L. Franke, Ink-bottle pore-method : Prediction of hygroscopic water content in hardened cement paste at variable climatic conditions, Cement and Concrete Research 36 (2006) 1954–1968.
- [3] K. K. Aligizaki, Pore Structure of Cement-Based Materials Testing Interpretation and Requirements - Modern Concrete Technology, Taylor & Francis, London, 2006.
- [4] K. Maekawa, R. Chaube, T. Kishi, Modelling of Concrete Performance : Hydration, Microstructure Formation and Mass Transport, E & FN Spon, London, 1999.
- [5] V. Baroghel-Bouny, Water vapour sorption experiments on hardened cementitious materials. Part I : Essential tool for analysis of hygral behaviour and its relation to pore structure, Cement and Concrete Research 37 (3) (2007) 414 – 437.
- [6] R. F. Feldman, Sorption and length-change scanning isotherms of methanol and water on hydrated portland cement, in : Proceedings of 5th International Congress on the Chemistry of Cement, vol. 3, Cement Association of Japan, Tokyo, Japan, 1968.
- [7] J.-P. Carlier, T. Rougelot, N. Burlion, Performance evaluation of models describing sorption isotherm in cementitious materials between saturation and oven dryness, Construction and Building Materials 37 (2012) 58–66.
- [8] B. Johannesson, M. Janz, A two-phase moisture transport model accounting for sorption hysteresis in layered porous building constructions, Building and Environment 44 (2009) 1285–1294.
- [9] H. Derluyn, D. Derome, J. Carmeliet, E. Stora, R. Barbarulo, Hysteretic moisture behavior of concrete : Modeling and analysis, Cement and Concrete Research 42 (2012) 1379–1388.

- [10] W. B. Haines, Studies in the physical properties of soil. v : The hysteresis effect in capillary properties, and the modes of moisture distribution associated therewith, *The Journal of Agricultural Science* 20 (1930) 97–116.
- [11] H. Q. Pham, D. G. Fredlund, S. L. Barbour, A study of hysteresis models for soil-water characteristic curves, *Canadian Geotechnical Journal* 42 (2005) 1548–1568.
- [12] A. Maqsoud, B. Bussiere, M. A. M. Mbonimpa, Hysteresis effects on the water retention curve : A comparison between laboratory results and predictive models, in : 57th Canadian Geotechnical Conference, Quebec, Canada, 2006.
- [13] A. Poulovassilis, Hysteresis of pore water, an application of concept of independent domains, *Soil Science* 93 (1962) 405–412.
- [14] F. Preisach, Über die magnetische nachwirkung, *Z. Physik* 94 (1935) 277–302.
- [15] L. Néel, Théorie des lois d'aimantation de lord rayleigh, *Cahiers de Physique* 13 (1943) 18–30.
- [16] D. H. Everett, A general approach to hysteresis - Part 3 : a formal treatment of the independent domain model of hysteresis, *Transactions of the Faraday Society* 50 (1954) 1077–1096.
- [17] D. H. Everett, A general approach to hysteresis - Part 4 : an alternative formulation of the domain model, *Transactions of the Faraday Society* 51 (1955) 1551–1557.
- [18] G. C. Topp, E. E. Miller, Hysteretic moisture characteristics and hydraulic conductivities for glass-bead media, *Soil Science Society of America Journal* 30 (1966) 156–162.
- [19] G. C. Topp, Soil-water hysteresis : The domain model theory extended to pore interaction conditions, *Soil Science Society of America Journal* 35 (1971) 219–225.
- [20] A. Poulovassilis, E. E. Childs, The hysteresis of pore water : the non-independence of domains, *Soil Science* 112 (1971) 301–312.
- [21] J. R. Philip, Similarity hypothesis for capillary hysteresis in porous materials, *Journal of Geophysical Research* 69 (1964) 1553–1562.
- [22] Y. Mualem, Modified approach to capillary hysteresis based on a similarity hypothesis, *Water Resources Research* 9 (1973) 1324–1331.
- [23] Y. Mualem, A conceptual model of hysteresis, *Water Resources Research* 10 (3) (1974) 514–520.
- [24] G. Bertotti, I. Mayergoyz, *The Science of Hysteresis. Volume III*, Elsevier Inc., Amsterdam, 2006.
- [25] Y. Mualem, G. Dagan, Dependent domain model of capillary hysteresis, *Water Resources Research* 11 (3) (1975) 452–460.
- [26] Y. Mualem, E. E. Miller, A hysteresis model based on an explicit domain-dependence function, *Soil Science Society of America Journal* 43 (6) (1979) 1067–1073.
- [27] Y. Mualem, A modified dependent-domain theory of hysteresis, *Journal of Soil Science* 137 (5) (1984) 283–291.
- [28] P. Lehmann, F. Stauffer, C. Hinze, O. Durya, H. Flüßler, Effect of hysteresis on water flow in a sand column with a fluctuating capillary fringe, *Journal of Contaminant Hydrology* 33 (1998) 81–100.
- [29] R. J. Hanks, A. Klute, E. Bresler, A numerical method for estimating infiltration, redistribution, drainage and evaporation of water from soil, *Water Resources Research* 5 (1969) 1064–1069.
- [30] D. Jaynes, Comparison of soil-water hysteresis models, *Journal of Hydrology* 75 (1984) 287–299.

- [31] P. S. Scott, G. J. Farquhar, N. Kouwen, Hysteresis effects on net infiltration, in : Advances in infiltration : Proceedings of the National Conference on Advances in Infiltration, Hyatt Regency Illinois Center, Chicago, Illinois, USA, 1983.
- [32] X. S. Li, Modelling of hysteresis response for arbitrary wetting-drying paths, *Computers and Geotechnics* 32 (2005) 133–137.
- [33] C. Wei, M. M. Dewoolkar, Formulation of capillary hysteresis with internal state variables, *Water Resources Research* 42 (2006) W07405.
- [34] U. Nyman, P. Gustafsson, B. Johannesson, R. Hagglund, A numerical method for the evaluation of non-linear transient moisture flow in cellulosic materials, *International Journal for Numerical Methods in Engineering* 66 (2006) 1859–1883.
- [35] B. Johannesson, P. Utgenannt, Microstructural changes caused by carbonation of cement mortar, *Cement and Concrete Research* 31 (2001) 925–931.
- [36] M. S. Ahs, Sorption scanning curves for hardened cementitious materials, *Construction and Building Materials* 22 (2008) 2228–2234.
- [37] K. Kosugi, Lognormal distribution model for unsaturated soil hydraulic properties, *Water Resources Research* 32 (1996) 2697–2703.
- [38] M. T. van Genuchten, A closed-form equation for predicting the hydraulic conductivity of unsaturated soils, *Soil Science Society of America Journal* 44 (1980) 892–898.
- [39] M. Mainguy, O. Coussy, V. Baroghel-Bouny, Role of air pressure in drying of weakly permeable materials, *Journal of Engineering Mechanics* 127 (2001) 582–592.
- [40] S. Poyet, S. Charles, N. Honoré, V. L’hostis, Assessment of the unsaturated water transport properties of an old concrete : Determination of the pore-interaction factor, *Cement and Concrete Research* 41 (2011) 1015–1023.
- [41] M. Feng, D. G. Fredlund, Hysteretic influence associated with thermal conductivity sensor measurements, in : The 52nd Canadian Geotechnical Conference, Sask, Canada, 1999.
- [42] D. G. Fredlund, A. Xing, Equations for the soil-water characteristic curve, *Canadian Geotechnical Journal* 31 (1994) 521–532.
- [43] W. Durner, Hydraulic conductivity estimation for soils with heterogeneous pore structure, *Water Resources Research* 30 (1994) 211–233.
- [44] H. Q. Pham, D. G. Fredlund, S. L. Barbour, A practical hysteresis model for the soil-water characteristic curve for soils with negligible volume change, *Geotechnique* 53 (2003) 293–298.
- [45] W. Brutsaert, Probability laws for pore-size distribution, *Soil Science* 101 (1966) 85–92.
- [46] R. H. Brooks, A. T. Corey, Hydraulic properties of porous media, Hydrology paper number 3, Colorado State University, Fort Colilins, Colo., 1964.
- [47] O. Ippisch, H.-J. Vogel, P. Bastian, Validity limits for the van genuchten–muallem model and implications for parameter estimation and numerical simulation, *Advances in Water Resources* 29 (2006) 1780–1789.
- [48] Y. Mualem, Prediction of the soil boundary wetting curve, *Journal of Soil Science* 137 (6) (1984) 379–390.
- [49] J.-Y. Parlange, Capillary hysteresis and the relationship between drying and wetting curves, *Water Resources Research* 12 (1976) 224–228.
- [50] R. D. Braddock, J.-F. Parlange, H. Lee, Application of a soil water hysteresis model to simple water retention curve, *Transport in Porous Media* 44 (2001) 407–420.

- [51] Y. Mualem, Extension of the similarity hypothesis used for modelling the soil water characteristics, *Water Resources Research* 13 (4) (1977) 773–780.
- [52] P. Viane, H. Vereecken, J. Diels, J. Feyen, A statistical analysis of six hysteresis models for the moisture retention characteristic, *Journal of Soil Science* 157 (1994) 345–355.
- [53] B. C. Si, R. C. Kachanoski, Unified solution for infiltration and drainage with hysteresis : Theory and field test, *Soil Science Society of America Journal* 64 (2000) 30–36.
- [54] A. Izady, B. Ghahraman, K. Davari, Hysteresis : Phenomenon and modeling in soil- water relationship, *Iran Agricultural Research* 28 (2009) 47–63.
- [55] Y. F. Dafalias, Bounding surface plasticity. i : Mathematical foundation and hypoplasticity, *Journal of Engineering Mechanics* 9 (1986) 966–987.
- [56] W. L. Hogarth, J. Hopmans, J.-Y. Parlange, R. Haverkamp, Application of a simple soil-water hysteresis model, *Journal of Hydrology* 98 (1988) 21–29.
- [57] H. Huang, Y. Tan, C. Liu, C. Chen, A novel hysteresis model in unsaturated soil, *Hydrological Processes* 19 (2005) 1653–1665.
- [58] J. Rubin, Numerical method for analyzing hysteresis-affected, post-infiltration redistribution of soil moisture, *Soil Science Society of American Process* 31 (1) (1967) 13–20.
- [59] A. D. Werner, D. A. Lockington, Artificial pumping errors in the Kool-Parker scaling model of soil moisture hysteresis, *Journal of Hydrology* 325 (2006) 118–133.
- [60] J. C. Parker, R. J. Lenhard, A model for hysteretic constitutive relations governing multiphase flow : 1. saturation-pressure relations, *Water Resources Research* 23 (1987) 2187–2196.
- [61] V. Baroghel-Bouny, M. Thiery, X. Wang, Modelling of isothermal coupled moisture-ion transport in cementitious materials, *Cement and Concrete Research* 41 (2011) 828–841.
- [62] V. Baroghel-Bouny, X. Wang, M. Thiery, M. Saillio, F. Barberon, Prediction of chloride binding isotherms of cementitious materials by analytical model or numerical inverse analysis, *Cement and Concrete Research* 42 (2012) 1207–1224.

TABLE 1: Proposed multi-level models of hysteresis.

Levels	Available experimental data	Description
Level 1	Both main branches and one scanning curve for each drying and wetting process	One scanning curve is used to determine parameters.
Level 2	Both main branches	Predicting scanning loops without additional parameters
Level 3	One main branch	Determining the other main branch and then predicting scanning loops

TABLE 2: Collected datasets of WVSIs measured by the saturated salt solution method [5].

No.	Name	Materials	Binders	W/C (W/B)
1	Concrete1	Concrete	OPC	0.45
2	Concrete2	Concrete	OPC+10%SF <sup>a</sup>	0.27 (0.24)
3	Concrete3	Concrete	OPC	0.43
4	Paste1	Paste	OPC	0.45
5	Paste2	Paste	OPC+10%SF <sup>a</sup>	0.20 (0.18)
6	Paste3	Paste	OPC	0.35
7	Paste4	Paste	OPC	0.45
8	Paste5	Paste	OPC	0.60

<sup>a</sup>. Silica fume.